IEEE Access
Multidisciplinary ⋮ Rapid Review ⋮ Open Access Journal

Received 8 June 2024, accepted 20 June 2024, date of publication 25 June 2024, date of current version 8 July 2024.

Digital Object Identifier 10.1109/ACCESS.2024.3419009

APPLIED RESEARCH

Real-Time Predicting the Low-Temperature Performance of WLTC-Based Lithium-Ion Battery Using an LSTM-PF Sequential Ensemble Model

MIN-SUNG SIM[1], DO-YOON KIM[1], YONG-JIN YOON[2], SEOK-WON KANG[1], AND JONG DAE BAEK[1]

[1]Department of Automotive Engineering, Yeungnam University, Gyeongsan, Gyeongbuk 38541, Republic of Korea
[2]Department of Mechanical Engineering, Korea Advanced Institute of Science and Technology (KAIST), Daejeon 34141, Republic of Korea

Corresponding authors: Seok-Won Kang (swkang@yu.ac.kr) and Jong Dae Baek (jdbaek@yu.ac.kr)

This work was supported by Korea Institute of Energy Technology Evaluation and Planning (KETEP) grant funded by the Korea government (MOTIE) (20214000000010, Gyeongbuk Regional Wind Energy Cluster Human Resources Development Project).

ABSTRACT Predicting an abnormally rapid decline in battery capacity in low-temperature environments is important for maintaining battery stability and performance. This study introduces a method that integrates cycling tests under various current conditions with deep neural network algorithms to identify and predict in real-time the trend of battery capacity reduction in low-temperature conditions (−10 °C). For this method, 18 feature data points were included, consisting of the test environment and conditions, as well as geometric and statistical features. The importance of these features was analyzed using the Random Forest (RF) algorithm, and the top 12 feature data points were selected to improve the efficiency and accuracy of the Long Short-Term Memory (LSTM) model. Furthermore, we applied a sequential ensemble technique that uses the output of the LSTM model as the input for the particle filter, significantly improving the performance of the prediction model. The approach was used to predict the capacity of the tested battery using C-rate transformation based on the WLTC. The results showed an error rate of 0.9% and an RMSE of 0.0048, representing a 25% decrease in the error rate and a 48% reduction in the RMSE compared with those predicted by the LSTM model.

INDEX TERMS Lithium-ion battery, low-temperature, long short-term memory (LSTM), particle filter (PF), worldwide light vehicles test cycle (WLTC), real-time prediction.

I. INTRODUCTION

Various studies are underway to achieve low-carbon goals using eco-friendly transportation methods. Electric vehicles (EVs), that use electric motors are being actively researched because they rely on battery packs instead of combustion engines [1], [2]. As the demand for electricity has surged, the need for stability and reliability has also increased. This makes fault diagnosis and battery pack monitoring crucial for enhancing safety, preventing cell damage, and ensuring optimal efficiency [3].

Lithium-ion batteries, which are known for their high energy density, high output voltage, low self-discharge, and minimal voltage drop, are used in various fields such as telecommunications, home appliances, energy storage devices, EVs, and aerospace [4], [5], [6]. These batteries begin to degrade immediately after production, necessitating their replacement when their capacity falls below 80% of the initial level [7], [8], [9]. Despite continuous improvements in performance and safety, lithium-ion batteries still pose risks of malfunction owing to aging, making precise monitoring of

The associate editor coordinating the review of this manuscript and approving it for publication was Xiao-Sheng Si.

the capacity degradation process and remaining life predictions vital. Batteries are particularly sensitive to temperature; typically, energy (discharge capacity) and power (operating voltage) significantly decrease at temperatures below −10 °C [10], [11], [12], [13], [14], highlighting the importance of accurate life prediction and stability maintenance under such abnormal performance drops. Ongoing studies have focused on battery characteristics, such as the dependence of the remaining capacity on the discharge rate and internal temperature, as well as cyclic aging phenomena.

Because of the nonlinear degradation of lithium-ion batteries, theoretical models based on experimentally measured data struggle to accurately predict the Remaining Useful Life (RUL) [15]. Accurate RUL prediction requires consideration of various internal and external conditions in addition to capacity [16]. Traditional RUL prediction methods utilize impedance measurements to analyze the relationship between internal resistance and aging and estimate the lifetime based on frequency-dependent impedance [17]. Although it is effective, this method requires battery removal from the system and costly electrochemical impedance spectroscopy (EIS) equipment. For this reason, an online battery impulse measurement technology has been introduced. The online battery impedance measurement system can continuously track the RUL, SOH, equivalent circuit parameters, etc. without the need for expensive equipment [18], [19]. Data-based analysis relies on neural networks to describe performance degradation and learn patterns from inception to failure, depending solely on the degradation data used for the explanation. Filtering models such as the Kalman Filter (KF) and Particle Filter (PF) employ Bayesian theory-based adaptive learning algorithms to predict RUL [20], [21], [22], [23], [24], [25], [26]. Nuhic [27] utilized a support vector machine (SVM) to estimate the battery State of Health (SoH) and RUL, and Nuhic [28] used (Relevance Vector Machine) to develop a capacity degradation model for RUL estimation. Recent advancements in deep learning have significantly enhanced neural network training capabilities [29]; employed a deep neural network (DNN) to encode time-dependent dependencies in state of charge (SoC) values, enabling accurate SoC estimation. Furthermore, deep convolutional neural networks (DCNNs) have shown higher accuracy and robustness in cell-level capacity prediction than traditional machine learning methods such as RVM [30]. Long Short-Term Memory (LSTM) RNN [31] captures long-term dependencies in performance degradation by optimizing the process using backpropagation over time. However, LSTM alone has limitations in predicting the trends of irregular battery capacities. Therefore, a combination of LSTM with other models has been proposed [32], [33]. In particular, the combination of LSTM with PF can effectively manage inherent noise and establish a probabilistic estimation framework, addressing LSTM's potential overfitting to historical trends when confronted with unusual data. This approach not only enhances prediction accuracy in the presence of data irregularities but also improves the reliability of state estimates under dynamic and uncertain operating conditions [34], [35]. In this study, we employed the LSTM-PF sequential ensemble model to create a hybrid prediction framework, significantly enhancing the reliability of remaining useful life (RUL) predictions for batteries under realistic variable conditions, thereby demonstrating the utility of this model in low-temperature environments.

TABLE 1. Samsung 18650 cell specifications used in the test.

Nominal Open Circuit Voltage	3.63 V
Min / Max Voltage	2.75 V / 4.2 V
Capacity	2600 mAh
Mass	45g

TABLE 2. Equipment specifications used for cycling tests.

Cycler Model	WBCS3000S (WonA Tech)
Test Channel Used	5 A, ±5 V Channel
Voltage / Current Accuracy	±0.02% / ±0.05% Full Scale
Thermal Chamber Model	TH3-KE-100 (Jeio Tech)
Temperature Range	-40 °C – 150 °C
Fluctuation	±0.3 °C

TABLE 3. Cycling test protocol.

Step No.	State	Condition	Cut-off
1	Charging (CC)	1C	≥4.2 V
2	Charging (CV)	4.2 V	≤250 mA
3	Rest	-	≥30 min
4	Discharging (CC)	1C	≤2.75 V
5	Rest	-	≥30 min

In this study, we conducted charge and discharge tests on lithium-ion batteries under low-temperature conditions, varying the current-rate (C-rate) from 0.5 C to 1.5 C in increments of 0.1 C. Test data were collected after each cycle. Eighteen variables were selected by extracting four test conditions: electrochemical properties, six geometric features related to battery deterioration owing to increased internal resistance during continuous charging and discharging, and eight statistical features related to voltage. These variables were divided into training and test datasets to train an ensemble model comprising the model and a particle filter. The trained ensemble model was designed to predict battery capacity degradation in the test data in real time by converting the speed specifications of the Worldwide Harmonized Light Vehicle Test Cycle (WLTC) international driving regulations into C-rates.

II. TEST AND METHODS

A. LITHIUM-ION BATTERY CYCLING TEST

1) CYCLING EQUIPMENT AND TEST PROCESS

The cells used in the experiment were Samsung 18650 lithium-ion batteries containing NMC (Nickel, Mn, and Cobalt) with a capacity of 2600 mAh. These cells have a

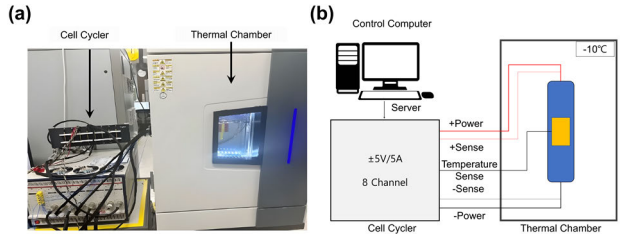

FIGURE 1. (a) Cell cycler and thermal chamber used in battery cycling test; (b) Test bench and system circuit diagram.

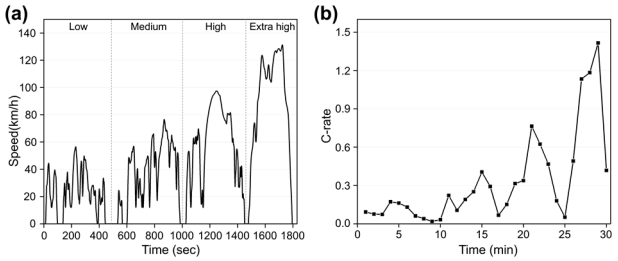

FIGURE 2. (a) WLTC Profile (Class 3); (b) C-rate converted by applying the vehicle assumed in the WLTC profile.

TABLE 4. Assumed vehicle specifications with WLTC driving.

Vehicle Mass	1500 kg
Battery Capacity	25 kWh
Nominal Voltage	350 V
Frontal Area	2.7 m^2

diameter of 18.0 mm and a length of 65.0 mm and are used globally. They were tested similarly to the cells previously used in Tesla vehicles. Detailed information about the batteries is presented in Table 1, and the specifications of all test equipment used in the cycling experiments are listed in Table 2. As indicated in Figures 1a and 1b, experiments were conducted using a cell cycler (WonATech) and a constant temperature and humidity chamber from Jeio Tech.

In cycling tests, the environment and conditions significantly affect battery degradation. In this study, the test environment was set to a temperature of −10 °C, under which the cycling tests were conducted. Additionally, as part of the test conditions, the charge-discharge C-rate was set, and tests were carried out at increments of 0.1C from 0.5C to 1.5C. The protocol used for the cycling tests, shown in Table 3, involved charging and discharging under a constant current–constant voltage (CC–CV), and a rest period of 30 min was provided after the completion of each charging and discharging cycle.

2) CYCLING TEST AND DATASETS BASED ON THE WLTC PROFILE

The WLTC is an automotive driving cycle included in the Worldwide Harmonized Light Vehicle Test Procedure (WLTP), agreed upon by the participating countries of the United Nations Economic Commission for Europe (UNECE) to measure fuel efficiency and pollutant emissions. This profile, developed based on real road traffic data collected from over 400 vehicles, has replaced the theoretically designed New European driving cycle (NEDC) since the 1980s, starting from 2018 [36]. The driving cycle includes three different cycle periods, Classes 1–3, applied according to the vehicle class defined by the output, with most general vehicles currently falling into Class 3. The cycle used for testing was Class 3, which was divided into four driving modes (low, medium, high, and extra-high) over 30 min, with each mode classified according to the maximum speed (Fig. 3a). Vehicles were assumed to be based on the WLTC to test the predicted battery capacity, and cycling tests were performed by calculating the C-rate (Table 4). Therefore, 12 cells were used for the test (WLTC001-012). The applied C-rate for the test protocol was averaged at 1-min intervals to ensure the stability of the cycling equipment (Fig. 3b). Detailed information about the hypothetical electric vehicle used for converting WLTC into C-rates is presented in Table 4.

B. ALGORITHM DESIGN

1) EXTRACT FEATURE DATA

To predict the discharge capacity of batteries in various cycles, it is essential to obtain feature data representing battery performance throughout the cycling process. Figures 3a and 3b show the voltage changes during charging and discharging, respectively, across cycles. As the cycle count increased, changes in the voltage curve were observed, owing to battery degradation. Although the general form of the voltage change remained similar throughout the cycles, the length of each cycle shortened, and the overall performance degraded as the battery discharge capacity decreased due to degradation. In this study, feature data (Table 5) used for model training was extracted based on the results of cycling tests conducted at −10 °C. The data included voltage changes (CVD, DVD) and battery temperature (CT, DT), and geometric analysis was utilized to extract features such as the initial rise and fall slopes of voltage (CVS, DVS), lengths of charge-discharge state (LC, LD), and slopes of load (CLS, DLS) (Fig. 3). The average (CAV and DAV), variance (CVV and DVV), skewness (CSV and DSV), and kurtosis (CKV and DKV) of the voltage were included as feature data, and statistical properties were used to extract the distribution and shape of the voltage in the data (Fig. 4).

2) LSTM-PF SEQUENTIAL ENSEMBLE MODEL

The recurrent neural network (RNN) is a model designed for processing time-series data, where the output values (hidden values) from a previous moment (layer) propagate to the next moment (layer), inheriting past information to process the time-series data. RNNs, through their recurrent mechanism that captures and remembers information from previous steps, have improved performance in learning time-series data compared to 'Feed forward' neural networks, where data flow in only one direction. However, during the gradient propagation process, the passage through the tanh operations can lead to vanishing gradients, where the gradient of the

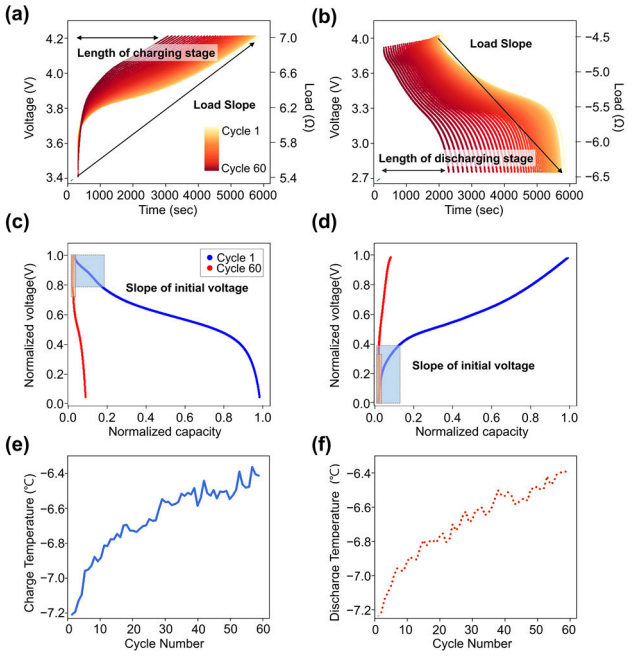

FIGURE 3. Feature data extracted by cycling tests: (a) Changes in voltage, load, and length of the charging section for 60 cycle; (b) Voltage and load during discharging, length of discharging section; (c) Initial slope of voltage to capacity in cycle 1 (blue) and cycle 60 (red) during chargin; (d) Initial slope of voltage to capacity in cycle 1 (blue) and cycle 60 (red) during dischargin; (e) Battery temperature change during chargin; (f) Battery temperature change during discharging.

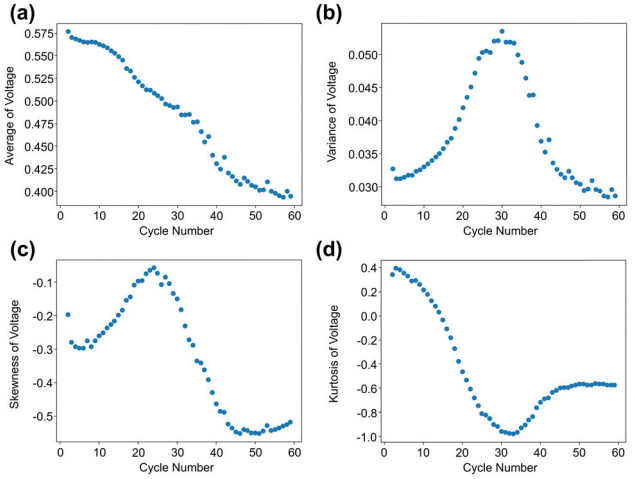

FIGURE 4. Statistical features of voltage during discharging: (a) Average of voltage; (b) Variance of voltage; (c) Skewness of voltage; (d) Kurtosis of voltage.

loss function becomes progressively smaller over time during training. To solve the problem of the gradient vanishing observed in conventional RNNs, LSTM was introduced [37], [38]. LSTM has three gates (input, forget, and output) that control the flow of information (Fig. 5).

The input gate is responsible for memorizing new information by receiving the current input and applying corresponding weight parameters, which are then passed through a Sigmoid (σ) activation function. The computational formula

TABLE 5. Extracted feature data for battery capacity prediction.

No.	Feature	State	No.	Feature	State
1	Voltage difference (CVD)	Charge	10	Voltage difference (DVD)	Discharge
2	Temperature (CT)		11	Temperature (DT)	
3	Initial voltage slope (CVS)		12	Initial voltage slope (DVS)	
4	Length of charge (LC)		13	Length of discharge (LD)	
5	Load slope (CLS)		14	Load slope (DLS)	
6	Average of voltage (CAV)		15	Average of voltage (DAV)	
7	Variance of voltage (CVV)		16	Variance of voltage (DVV)	
8	Skewness of voltage (CSV)		17	Skewness of voltage (DSV)	
9	Kurtosis of voltage (CKV)		18	Kurtosis of voltage (DKV)	

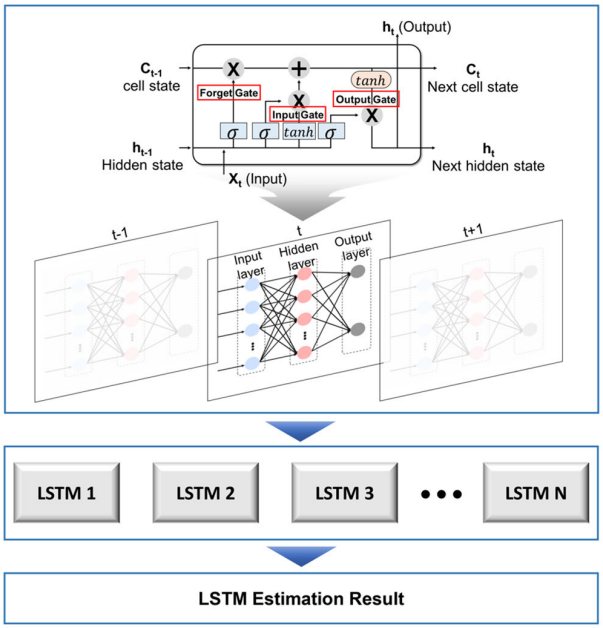

FIGURE 5. LSTM model structure.

is as follows:

$$i_t = \sigma(W_i \times [h_{t-1}, x_t] + b_i) \tag{1}$$

The hidden state (h_{t-1}) is combined with the input (x_t) and multiplied by the weight parameter (W_i), after which a bias (b_i) is added. The weight parameters and bias are parameters learned by the model, which determine the importance of the input and previous hidden states, respectively, and adjust the activation of the gate. Finally, the value with the applied weights is passed through the Sigmoid activation function (σ). The Sigmoid function limits the output values between 0 and 1, where values closer to 1 determine how much information will be added to the cell state; this is referred to as the output of the input gate (i_t). Each gate in LSTM follows

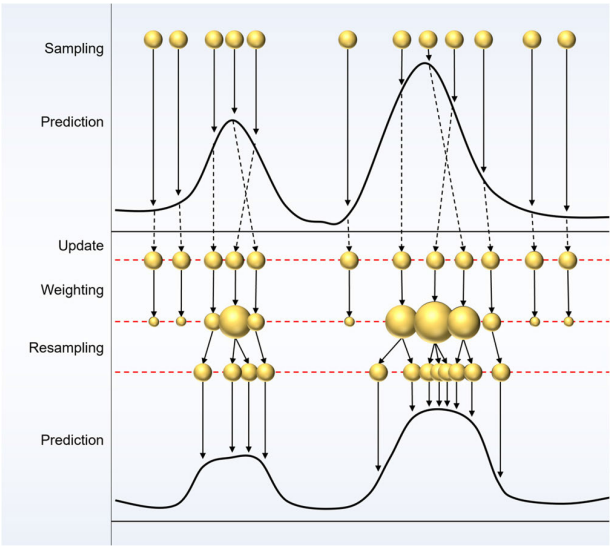

FIGURE 6. Particle filter proces.

a common computational paradigm but performs different functions with parameters adjusted according to their roles.

Furthermore, the forget gate is a key component of the LSTM that decides whether to retain or discard previous information in the cell. This allows the LSTM to effectively remove unnecessary information and maintain only the required information, thereby enabling it to learn long-term dependencies in sequential data. The computational formula is as follows:

$$f_t = \sigma(W_f \times [h_{t-1}, x_t] + b_f) \tag{2}$$

Finally, the output gate receives the current input and outputs the final output value, or next hidden value (h_t). Through this process, the LSTM can extract important information from sequence data and learn complex patterns and dependencies based on this information. The computational formula is as follows:

$$o_t = \sigma(W_o \times [h_{t-1}, x_t] + b_o) \tag{3}$$

To increase the generalization performance under various conditions, the proposed model is a multi-LSTM algorithm that learns using a dataset classified according to the current conditions and outputs the predicted capacity value of the final LSTM.

The PF is used to estimate the system states and is particularly effective in nonlinear systems where the relationship between the system's states and observations is complex [39], [40]. The PF process involves randomly generating particles and predicting the state of each particle using the system model, allowing the addition of noise considering the uncertainty in the process model as the particles are updated. The particles are evaluated based on how well they explain the observations, and initial weights are assigned, typically normalized so that their sum is equal to one. Particles with lower weights are discarded, whereas those with higher weights are replicated for a more accurate estimation. An improved state estimation was performed when the particle set was updated (Fig. 6).

By sequentially ensembling the LSTM with the PF, a mechanism is used in which the output values of the LSTM are utilized as input values for the PF. In this model, the main prediction of battery capacity was performed using LSTM, and a particle filter was used to enhance the generalization performance of LSTM. This allows the LSTM to learn long-term patterns and dependencies from sequence data for state prediction, whereas the PF applies a probabilistic modeling layer considering the uncertainty and noise in these predictions. Thus, it provides more precise state estimation. The ensemble model performed real-time predictions by replacing the capacity predicted in the previous cycle with the actual collected capacity when predicting capacity. The results predicted by this ensemble model were assessed by calculating the root mean squared error (RMSE), mean absolute percentage error (MAPE) and average error rate throughout the cycle. The RMSE represents the root mean square error between the actual and predicted values of the model, with a lower RMSE generally indicating a higher prediction accuracy. MAPE represents the percentage of errors, which can be interpreted independently and intuitively on the scale.

$$RMSE = \sqrt{\frac{1}{N}\sum_i^N (pred_i - target_i)^2} \tag{4}$$

$$MAPE = \frac{1}{N}\sum_i^N \left|\frac{pred_i - target_i}{pred_i}\right| \times 100\% \tag{5}$$

3) DATASET PARTITIONING FOR TRAINING, VALIDATION, AND TEST

Data partitioning is essential to construct a model with good generalization performance [41]. The data should be divided into training data for the model to learn, validation data for calibration, and test data for evaluation to prevent overfitting and build a model with superior generalization performance. Generalization performance refers to the ability of a model trained on training data to predict external data that are not included in the training set. The better the generalization performance, the better the constructed model, which requires choosing learning techniques, datasets, and fine-tuning detailed parameters. In this study, the dataset from the cycling test results comprised 55 data points, from B_001 to B_055, with each current condition divided into 60% training data, 20% validation data, and 20% test data (Table 6).

4) USING TECHNIQUES FOR EFFICIENT PREDICTIVE MODELING

Random forest is a widely used machine learning method for building predictive models. Reducing the number of variables is important to reduce the burden of data collection and increase the efficiency of predictive modeling [42]. The random forest course first learns the dataset, and then evaluates

TABLE 6. Cycling test datasets to be used for training, validation, and test.

Dataset	C-rate	Cycle	Note
B_001 – B_003	0.5	80	Training
B_004			Validation
B_005			Test
B_006 – B_008	0.6		Training
B_009			Validation
B_010			Test
B_011 – B_013	0.7		Training
B_014			Validation
B_015			Test
B_016 – B_018	0.8		Training
B_019			Validation
B_020			Test
B_021 – B_023	0.9		Training
B_024			Validation
B_025			Test
B_026 – B_028	1.0		Training
B_029			Validation
B_030			Test
B_031 – B_033	1.1		Training
B_034			Validation
B_035			Test
B_036 – B_038	1.2	60	Training
B_039			Validation
B_040			Test
B_041 – B_043	1.3		Training
B_044			Validation
B_045			Test
B_046 – B_048	1.4		Training
B_049			Validation
B_050			Test
B_051 – B_053	1.5		Training
B_054			Validation
B_055			Test

Voltage(V): 4.2/2.75, Temp(℃): -10

the importance of each variable. We selected a variable of high importance and discarded the remaining variables. The model was then re-learned using the selected variables, and its performance was evaluated (Fig. 7). In this study, a random forest was used to evaluate the importance of the variables on the capacity of the battery, and variables with high importance were selected.

Cross-validation is considered one of the most important tools for evaluating regression and classification methods [43]. The reason for using cross-validation is that it provides more datasets for training and testing than classifying into groups of datasets only, which is advantageous for

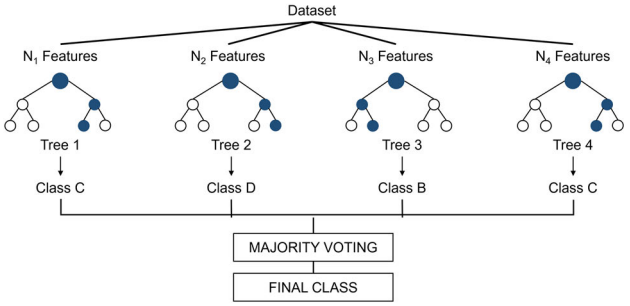

FIGURE 7. Random forest classification process.

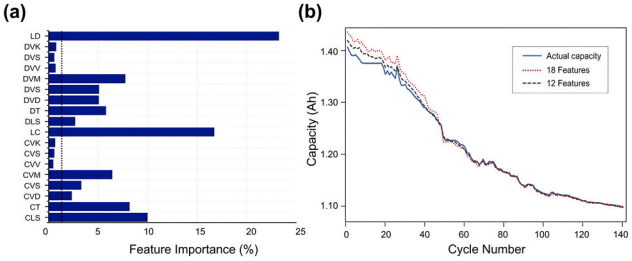

FIGURE 8. a) The evaluation results of feature data importance using Random Forest and dashed line indicates 1%; (b) Comparison of prediction error rates based on variable selection.

increasing the accuracy in cases where data are limited. In this study, rolling window cross-validation (RWCV) was used to compensate for accuracy issues caused by data scarcity. This method involves a fixed-size window moving at a constant step size and repeating training and testing, thereby offering advantages in predicting time-series data.

III. RESULTS

A. DETERMINING FEATURE DATA FOR MODEL TRAINING

Using Random Forest, we evaluated the importance of the existing 18 feature data points for battery capacity. The results indicated that the lengths of the charge and discharge segments were the most crucial factors. Because the importance of the voltage variance, kurtosis, and skewness was negligible (approximately 1 %), these features were excluded from the training. Consequently, the top 12 feature data points were used for training (Fig. 8a). When the model was trained using all 18 variables, the error rate was observed to be 1.1%. However, when trained with only the selected 12 variables, the error rate decreased to 0.9%, indicating an 18% improvement (Fig. 8b).

B. REAL-TIME CAPACITY PREDICTION BASED ON THE LSTM-PF SEQUENTIAL ENSEMBLE MODEL

To enhance the predictive performance of the LSTM model, the PF was applied as a sequential ensemble technique, utilizing the output of the LSTM as input for the PF. To verify the LSTM-PF sequential ensemble model, the tested battery capacity based on the WLTC was compared with the predicted result using the LSTM alone. The results of predicting the real-time capacity of 12 cells (WLTC001-012) are shown

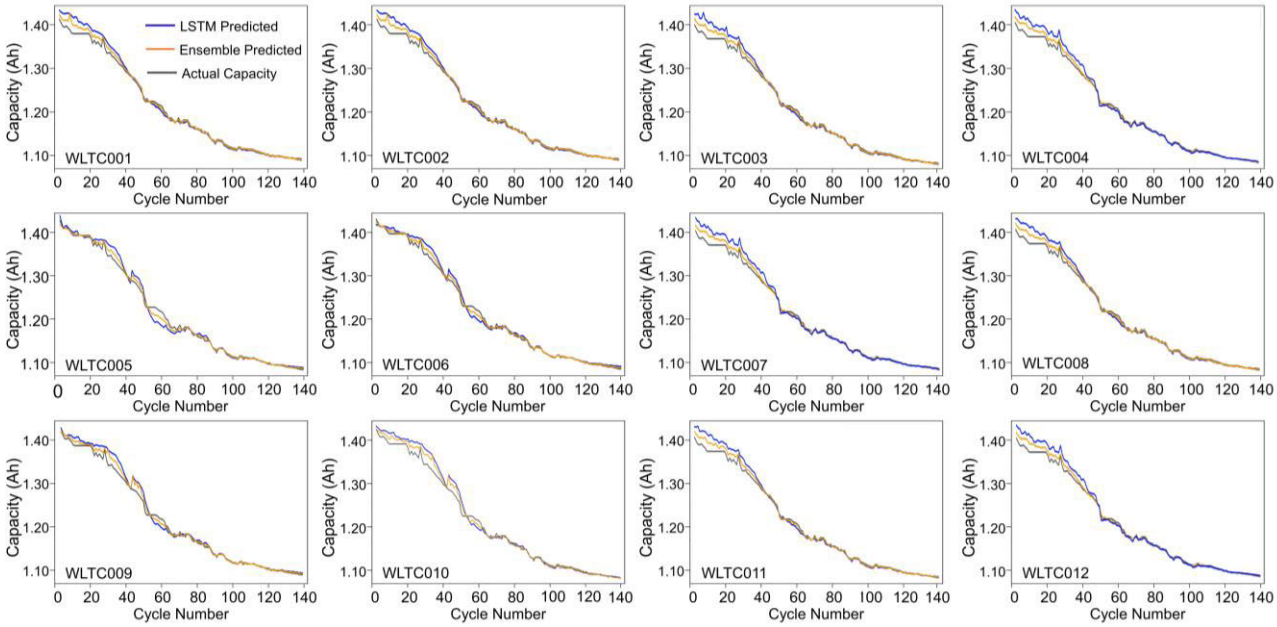

FIGURE 9. Prediction results of LSTM and LSTM-PF ensemble models for WLTC battery dataset.

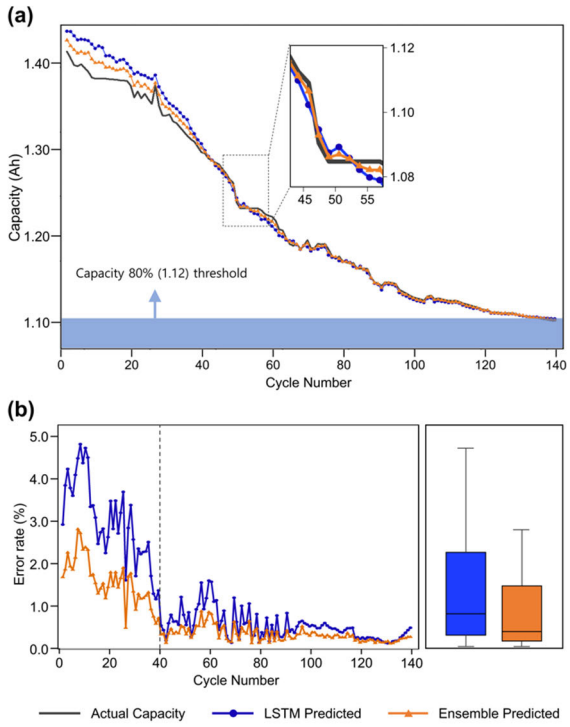

FIGURE 10. (a) The prediction results of battery capacity based on the LSTM-PF ensemble model; (b) The trend of error rate of LSTM and ensemble models by cycle and the box plot, dashed line indicates cycle 40.

in Fig. 9. The gray line indicates the actual battery capacity, the blue line indicates the prediction by the standalone LSTM model, and the orange line indicates the prediction by the LSTM-PF ensemble model. In all the cells, the ensemble model exhibited higher performance than the LSTM model. The RMSE, MAPE and error rates of the test cells are listed in Table 7.

Figure 10 shows the average predictions for the 12 cells. By applying the C-rate conversion based on the WLTC driving regulation, the battery was tested up to an 80% capacity threshold for approximately 140 cycles; the blue shade represents the 80% capacity threshold of the battery (1.12 Ah). At this point, the trained model predicts the capacity for the same number of cycles. Throughout the cycle, it was confirmed that the predicted values of the LSTM-PF ensemble model were closer to the actual capacity values than those of the standalone LSTM model. The ensemble model showed a higher prediction accuracy than the LSTM model during the 2.7% capacity decrease that occurred between cycles 45 and 50. Comparing the cell-average RMSE evaluation, the LSTM model showed 0.0092, whereas the LSTM-PF ensemble model showed 0.0048. The LSTM model showed a prediction error rate of 1.2%, whereas the ensemble model showed a prediction error rate of 0.9%. As the number of cycles increased, both models indicated that the error rate decreased. In particular, the error rate decreases significantly for up to 40 cycles.

IV. DISCUSSION

A. MODEL VALIDATION FOR REAL-TIME CAPACITY PREDICTION

The approach of combining LSTM and PF into a sequential ensemble is useful for improving the accuracy of the battery capacity trend prediction. The LSTM model is effective for recognizing time-dependent data patterns and learning long-term dependencies; however, it is limited to optimization within a fixed structure. Therefore, there are limitations to the predictive performance of LSTM for complex or noisy data.

TABLE 7. Comparison of predictive performance between LSTM models and ensemble models by cells.

Cell	RMSE (LSTM)	RMSE (Ensemble)	MAPE (LSTM)	MAPE (Ensemble)	Error rate (LSTM)	Error rate (Ensemble)
WLTC001	0.0090	0.0042	0.44%	0.22%	1.31%	0.89%
WLTC002	0.0091	0.0047	0.45%	0.21%	1.14%	0.92%
WLTC003	0.0099	0.0051	0.49%	0.23%	1.48%	1.13%
WLTC004	0.0097	0.0051	0.48%	0.25%	1.38%	0.97%
WLTC005	0.0079	0.0048	0.39%	0.25%	0.91%	0.73%
WLTC006	0.0081	0.0049	0.41%	0.24%	0.93%	0.76%
WLTC007	0.0098	0.0052	0.49%	0.25%	1.36%	1.01%
WLTC008	0.0092	0.0048	0.46%	0.24%	1.22%	0.88%
WLTC009	0.0089	0.0047	0.44%	0.23%	1.06%	0.87%
WLTC010	0.0101	0.0053	0.50%	0.26%	1.50%	1.24%
WLTC011	0.0093	0.0047	0.46%	0.23%	1.17%	0.87%
WLTC012	0.0094	0.0042	0.47%	0.21%	1.18%	0.88%

In this study, by combining the output values of LSTM as input values for PF, we were able to reduce the uncertainty in LSTM predictions and achieve high predictive performance, even with noisy data. When comparing the RMSE metrics of the models, the standalone LSTM model had an RMSE of 0.0092, whereas the ensemble model had an RMSE of 0.0048, indicating a 48% decrease compared to using LSTM alone. Additionally, when comparing the error rates, that of the LSTM model was 1.2%, whereas that of the LSTM-PF ensemble model was 0.9%, demonstrating a 25% lower error rate. As the number of cycles increases, the actual capacity data collected in real time become more abundant, resulting in a decrease in the prediction error rate. Notably, there was a significant reduction in the error rate for up to 40 cycles, which was 30 percent of the total number of cycles. This proves that most predictions regarding battery capacity are performed by the LSTM model; however, the PF model, which can improve the shortcomings of LSTM and update the probability distribution of the prediction results to supplement generalization performance, was successfully combined for complex systems.

B. SCALABILITY AND LIMITATIONS OF THE MODEL

This study demonstrated the ability to reflect the battery performance for actual driving regulations in low-temperature environments by predicting the battery capacity for the WLTC driving cycle using the LSTM-PF ensemble model. During the model training process, battery cycling test data under various current conditions were integrated to increase the versatility and scalability of the model. This approach can be extended to other battery technologies and various operational environments by capturing the complex system related to battery aging with high accuracy, without the need to detach the battery and measure the impedance with EIS.

However, the battery packs used in actual vehicles are composed of multiple cells and involve complex interactions, which can differ from the results of cycling tests based on a single cell. To overcome this limitation, future studies should conduct cycling tests at the battery pack level and develop prediction models that consider the interactions between various cells. Furthermore, incorporating variables related to complex electrical and thermal interactions can bring us closer to optimizing battery management systems in actual operating environments, thereby contributing to the overall performance and stability of EVs.

V. CONCLUSION

In this study, cycling tests were conducted, and a DNN model was designed to understand and predict real-time trends in battery capacity at low temperatures. From the results of the low-temperature cycling tests, 18 feature data points were extracted, including the test environment and conditions, geometric features, and statistical features. Important features for training were selected through analysis using Random Forest. The error rate improved by 18% from 1.1% to 0.9% when trained with the selected 12 variables. The prediction model combines the output of the LSTM as input for the PF using a sequential ensemble technique. The ensemble model accurately predicted (error rate: 0.9%, RMSE: 0.0048) the capacity of batteries tested with C-rate conversions according to WLTC driving regulations in real time, demonstrating a higher performance than using LSTM alone (error rate: 1.2%, RMSE: 0.0092).

Our research presents an approach for collecting datasets from lithium-ion batteries at low temperatures to analyze the low-temperature behavior characteristics of lithium-ion batteries and accurately predict abnormal decreases in battery capacity. We propose a higher-performance model because LSTM alone is limited in capturing all the complex battery capacity decline trends. The approach proposed in this study is expected to assist in the efficient use of batteries and prevention of accidents during battery use by accurately predicting the lifetime of lithium-ion batteries.

REFERENCES

[1] H. Dai, X. Wei, Z. Sun, J. Wang, and W. Gu, "Online cell SOC estimation of Li-ion battery packs using a dual time-scale Kalman filtering for EV applications," *Appl. Energy*, vol. 95, pp. 227–237, Jul. 2012, doi: 10.1016/j.apenergy.2012.02.044.

[2] A. Manthiram, "An outlook on lithium ion battery technology," *ACS Central Sci.*, vol. 3, no. 10, pp. 1063–1069, Oct. 2017, doi: 10.1021/acscentsci.7b00288.

[3] J. Rivera-Barrera, N. Muñoz-Galeano, and H. Sarmiento-Maldonado, "SoC estimation for lithium-ion batteries: Review and future challenges," *Electronics*, vol. 6, no. 4, p. 102, Nov. 2017, doi: 10.3390/electronics6040102.

[4] M. Li, J. Lu, Z. Chen, and K. Amine, "30 years of lithium-ion batteries," *Adv. Mater.*, vol. 30, no. 33, Aug. 2018, Art. no. 1800561, doi: 10.1002/adma.201800561.

[5] T. Kim, W. Song, D.-Y. Son, L. K. Ono, and Y. Qi, "Lithium-ion batteries: Outlook on present, future, and hybridized technologies," *J. Mater. Chem. A*, vol. 7, no. 7, pp. 2942–2964, 2019, doi: 10.1039/c8ta10513h.

[6] T. M. Bandhauer, S. Garimella, and T. F. Fuller, "A critical review of thermal issues in lithium-ion batteries," *J. Electrochem. Soc.*, vol. 158, no. 3, p. R1, 2011, doi: 10.1149/1.3515880.

[7] C. Heymans, S. B. Walker, S. B. Young, and M. Fowler, "Economic analysis of second use electric vehicle batteries for residential energy storage and load-levelling," *Energy Policy*, vol. 71, pp. 22–30, Aug. 2014, doi: 10.1016/j.enpol.2014.04.016.

[8] L. C. Casals, B. Amante García, and C. Canal, "Second life batteries lifespan: Rest of useful life and environmental analysis," *J. Environ. Manage.*, vol. 232, pp. 354–363, Feb. 2019, doi: 10.1016/j.jenvman.2018.11.046.

[9] H.-C. Chung, "Charge and discharge profiles of repurposed $LiFePO_4$ batteries based on the UL 1974 standard," *Sci. Data*, vol. 8, no. 1, p. 165, 1974, doi: 10.6084/m9.figshare.14495604.

[10] R. Kumar and V. Goel, "A study on thermal management system of lithium-ion batteries for electrical vehicles: A critical review," *J. Energy Storage*, vol. 71, Nov. 2023, Art. no. 108025, doi: 10.1016/j.est.2023.108025.

[11] S. Chen, X. Wei, G. Zhang, X. Wang, J. Zhu, X. Feng, H. Dai, and M. Ouyang, "All-temperature area battery application mechanism, performance, and strategies," *Innovation*, vol. 4, no. 4, Jul. 2023, Art. no. 100465, doi: 10.1016/j.xinn.2023.100465.

[12] X. Shi, G. Li, R. Zhang, O. C. Esan, X. Huo, Q. Wu, and L. An, "Operation of rechargeable metal-ion batteries in low-temperature environments," *Renew. Sustain. Energy Rev.*, vol. 189, Jan. 2024, Art. no. 113861, doi: 10.1016/j.rser.2023.113861.

[13] S. S. Zhang, K. Xu, and T. R. Jow, "A new approach toward improved low temperature performance of Li-ion battery," *Electrochem. Commun.*, vol. 4, no. 11, pp. 928–932, Nov. 2002, doi: 10.1016/S1388-2481(02)00490-3.

[14] G. Zhu, K. Wen, W. Lv, X. Zhou, Y. Liang, F. Yang, Z. Chen, M. Zou, J. Li, Y. Zhang, and W. He, "Materials insights into low-temperature performances of lithium-ion batteries," *J. Power Sources*, vol. 300, pp. 29–40, Dec. 2015, doi: 10.1016/j.jpowsour.2015.09.056.

[15] K. Liu, K. Li, Q. Peng, and C. Zhang, "A brief review on key technologies in the battery management system of electric vehicles," *Frontiers Mech. Eng.*, vol. 14, no. 1, pp. 47–64, Mar. 2019, doi: 10.1007/s11465-018-0516-8.

[16] W. Waag, C. Fleischer, and D. U. Sauer, "Adaptive on-line prediction of the available power of lithium-ion batteries," *J. Power Sources*, vol. 242, pp. 548–559, Nov. 2013, doi: 10.1016/j.jpowsour.2013.05.111.

[17] U. Tröltzsch, O. Kanoun, and H.-R. Tränkler, "Characterizing aging effects of lithium ion batteries by impedance spectroscopy," *Electrochim. Acta*, vol. 51, nos. 8–9, pp. 1664–1672, Jan. 2006, doi: 10.1016/j.electacta.2005.02.148.

[18] A. Guha and A. Patra, "Online estimation of the electrochemical impedance spectrum and remaining useful life of lithium-ion batteries," *IEEE Trans. Instrum. Meas.*, vol. 67, no. 8, pp. 1836–1849, Aug. 2018, doi: 10.1109/TIM.2018.2809138.

[19] S. M. R. Islam and S.-Y. Park, "Precise online electrochemical impedance spectroscopy strategies for Li-ion batteries," *IEEE Trans. Ind. Appl.*, vol. 56, no. 2, pp. 1661–1669, Mar. 2020, doi: 10.1109/TIA.2019.2958555.

[20] C. Hu, B. D. Youn, and J. Chung, "A multiscale framework with extended Kalman filter for lithium-ion battery SOC and capacity estimation," *Appl. Energy*, vol. 92, pp. 694–704, Apr. 2012, doi: 10.1016/j.apenergy.2011.08.002.

[21] J. Han, D. Kim, and M. Sunwoo, "State-of-charge estimation of lead-acid batteries using an adaptive extended Kalman filter," *J. Power Sources*, vol. 188, no. 2, pp. 606–612, Mar. 2009, doi: 10.1016/j.jpowsour.2008.11.143.

[22] G. L. Plett, "Extended Kalman filtering for battery management systems of LiPB-based HEV battery packs: Part 1," *J. Power Sources*, vol. 134, no. 2, pp. 252–261, Aug. 2004, doi: 10.1016/j.jpowsour.2004.02.031.

[23] G. L. Plett, "Extended Kalman filtering for battery management systems of LiPB-based HEV battery packs: Part 2," *J. Power Sources*, vol. 134, no. 2, pp. 262–276, Aug. 2004, doi: 10.1016/j.jpowsour.2004.02.032.

[24] G. L. Plett, "Extended Kalman filtering for battery management systems of LiPB-based HEV battery packs: Part 3," *J. Power Sources*, vol. 134, no. 2, pp. 277–292, Aug. 2004, doi: 10.1016/j.jpowsour.2004.02.033.

[25] Z. Chen, "Bayesian filtering: From Kalman filters to particle filters, and beyond," *Statistics*, vol. 182, pp. 1–69, Jan. 2003.

[26] Y. Zhang, R. Xiong, H. He, and Z. Liu, "A LSTM-RNN method for the lithuim-ion battery remaining useful life prediction," in *Proc. Prognostics Syst. Health Manage. Conf. (PHM-Harbin)*, Jul. 2017, pp. 1–4, doi: 10.1109/PHM.2017.8079316.

[27] A. Nuhic, T. Terzimehic, T. Soczka-Guth, M. Buchholz, and K. Dietmayer, "Health diagnosis and remaining useful life prognostics of lithium-ion batteries using data-driven methods," *J. Power Sources*, vol. 239, pp. 680–688, Oct. 2013, doi: 10.1016/j.jpowsour.2012.11.146.

[28] D. Wang, Q. Miao, and M. Pecht, "Prognostics of lithium-ion batteries based on relevance vectors and a conditional three-parameter capacity degradation model," *J. Power Sources*, vol. 239, pp. 253–264, Oct. 2013, doi: 10.1016/j.jpowsour.2013.03.129.

[29] E. Chemali, P. J. Kollmeyer, M. Preindl, and A. Emadi, "State-of-charge estimation of Li-ion batteries using deep neural networks: A machine learning approach," *J. Power Sources*, vol. 400, pp. 242–255, Oct. 2018, doi: 10.1016/j.jpowsour.2018.06.104.

[30] S. Shen, M. Sadoughi, X. Chen, M. Hong, and C. Hu, "A deep learning method for online capacity estimation of lithium-ion batteries," *J. Energy Storage*, vol. 25, Oct. 2019, Art. no. 100817, doi: 10.1016/j.est.2019.100817.

[31] Y. Zhang, R. Xiong, H. He, and M. G. Pecht, "Long short-term memory recurrent neural network for remaining useful life prediction of lithium-ion batteries," *IEEE Trans. Veh. Technol.*, vol. 67, no. 7, pp. 5695–5705, Jul. 2018, doi: 10.1109/TVT.2018.2805189.

[32] X. Li, L. Zhang, Z. Wang, and P. Dong, "Remaining useful life prediction for lithium-ion batteries based on a hybrid model combining the long short-term memory and Elman neural networks," *J. Energy Storage*, vol. 21, pp. 510–518, Feb. 2019, doi: 10.1016/j.est.2018.12.011.

[33] K. Park, Y. Choi, W. J. Choi, H.-Y. Ryu, and H. Kim, "LSTM-based battery remaining useful life prediction with multi-channel charging profiles," *IEEE Access*, vol. 8, pp. 20786–20798, 2020, doi: 10.1109/ACCESS.2020.2968939.

[34] X. Yan, G. Zhou, W. Wang, P. Zhou, and Z. He, "A hybrid data-driven method for state-of-charge estimation of lithium-ion batteries," *IEEE Sensors J.*, vol. 22, no. 16, pp. 16263–16275, Aug. 2022, doi: 10.1109/JSEN.2022.3188845.

[35] X. Hu, X. Yang, F. Feng, K. Liu, and X. Lin, "A particle filter and long short-term memory fusion technique for lithium-ion battery remaining useful life prediction," *J. Dyn. Syst., Meas., Control*, vol. 143, no. 6, Jun. 2021, Art. no. 061001, doi: 10.1115/1.4049234.

[36] M. Tutuianu, P. Bonnel, B. Ciuffo, T. Haniu, N. Ichikawa, A. Marotta, J. Pavlovic, and H. Steven, "Development of the world-wide harmonized light duty test cycle (WLTC) and a possible pathway for its introduction in the European legislation," *Transp. Res. D, Transp. Environ.*, vol. 40, pp. 61–75, Oct. 2015, doi: 10.1016/j.trd.2015.07.011.

[37] A. Sherstinsky, "Fundamentals of recurrent neural network (RNN) and long short-term memory (LSTM) network," *Phys. D, Nonlinear Phenomena*, vol. 404, Mar. 2020, Art. no. 132306, doi: 10.1016/j.physd.2019.132306.

[38] Y. Yu, X. Si, C. Hu, and J. Zhang, "A review of recurrent neural networks: LSTM cells and network architectures," *Neural Comput.*, vol. 31, no. 7, pp. 1235–1270, Jul. 2019, doi: 10.1162/neco_a_01199.

[39] P. M. Djuric, J. H. Kotecha, J. Zhang, Y. Huang, T. Ghirmai, M. F. Bugallo, and J. Miguez, "Particle filtering," *IEEE Signal Process. Mag.*, vol. 20, no. 5, pp. 19–38, Sep. 2003, doi: 10.1109/MSP.2003.1236770.

[40] J. Carpenter, P. Clifford, and P. Fearnhead, "Improved particle filter for nonlinear problems," *IEE Proc. - Radar, Sonar Navigat.*, vol. 146, no. 1, pp. 2–7, 1999, doi: 10.1049/ip-rsn:19990255.

[41] Y. Xu and R. Goodacre, "On splitting training and validation set: A comparative study of cross-validation, bootstrap and systematic sampling for estimating the generalization performance of supervised learning," *J. Anal. Test.*, vol. 2, no. 3, pp. 249–262, Jul. 2018, doi: 10.1007/s41664-018-0068-2.

[42] J. L. Speiser, M. E. Miller, J. Tooze, and E. Ip, "A comparison of random forest variable selection methods for classification prediction modeling," *Expert Syst. Appl.*, vol. 134, pp. 93–101, Nov. 2019, doi: 10.1016/j.eswa.2019.05.028.

[43] C. Bergmeir and J. M. Benítez, "On the use of cross-validation for time series predictor evaluation," *Inf. Sci.*, vol. 191, pp. 192–213, May 2012, doi: 10.1016/j.ins.2011.12.028.

MIN-SUNG SIM was born in Busan, South Korea, in 1994. He received the B.S. degree in integrated plant science from Chung-Ang University, Anseong, South Korea, in 2019, with a minor in plant physiology and molecular biology, and the M.S. degree in automotive engineering from Yeungnam University, Gyeongsan, South Korea, in 2024. He is currently pursuing the Ph.D. degree with the Department of Mechanical Engineering, Korea Advanced Institute of Science and Technology (KAIST), Daejeon, South Korea.

He published one in 2023 in a field related to geographic weighted regression. His research interests include battery diagnosis, battery lifetime prediction, machine learning, and artificial intelligence.

DO-YOON KIM was born in Daegu, South Korea, in 1998. He received the B.S. and M.S. degrees in automotive engineering from Yeungnam University, Gyeongsan, South Korea, in 2022 and 2024, respectively.

His research interests include predicting the electrochemical characteristics of lithium-ion batteries, predicting the degradation of PEMFC, and numerical methods in engineering. He is a member of the Korean Society of Mechanical Engineers (KSME), the Korean Electrochemical Society (KECS), and the Korean Society for Railway (KSR).

YONG-JIN YOON received the first M.S. degree in mechanical engineering, the second M.S. degree in electrical engineering, and the Ph.D. degree in mechanical engineering from Stanford University, CA, USA, in 2005, 2008, and 2009, respectively, with a minor in management science and engineering.

He is currently an Associate Professor with the Department of Mechanical Engineering, Korea Advanced Institute of Science and Technology (KAIST), the President of the University Industrial Technology Force (UNITEF), an Advisor of the KAIST Startup Center, the Director of the Advanced Drone Innovation Center, an Advisory Partner of Enlight Venture Capital, a Venture Partner of ES Investor, and a Visiting Professor of Nanyang Technological University. He has published more than 130 international journal articles (SCI indexed) and more than 170 international conference proceedings papers. His current research interests include 3D-printed biosensors, drone power sources using nano thin-film fabrication, and smart manufacturing for advanced nano drones.

SEOK-WON KANG received the M.S. degree in mechanical engineering from the Division of Aerospace Engineering, KAIST, Daejeon, South Korea, in 2007, and the Ph.D. degree in mechanical engineering from Texas A&M University, College Station, TX, USA, in 2012.

From 2007 and 2008, he was a Research Engineer with the Research and Development Division, Renault Samsung Motors, South Korea. After completing the Ph.D. degree, from 2012 to 2018, he was a Senior Researcher with the Metropolitan Transportation Research Center, Korea Railroad Research Institute, Uiwang, South Korea. He is currently an Associate Professor with the Department of Automotive Engineering, Yeungnam University, Gyeongsan, South Korea. He has 57 publications in SCIE-indexed journals as well as two book chapters in micro-electro-mechanical systems (MEMS), nano/micro-scale thermos-fluidics, and energy conversion/storage, since 2010. His research interests include the design of a MEMS sensor, microfluidics, nanophotonics, CNT nanoelectronics, green and intelligent vehicle systems, and numerical methods in engineering.

Dr. Kang is a member of the Korean Society of Mechanical Engineers (KSME), the Korean Society of Automotive Engineers (KSAE), the Korean Society for Railway (KSR), and the Korean Electrochemical Society (KECS).

JONG DAE BAEK received the M.S. degree in mechanical engineering from Stanford University, Stanford, CA, USA, and the Ph.D. degree in mechanical and aerospace engineering from Nanyang Technological University, in 2016. He completed his dissertation on the fabrication and characterization of low-temperature thin film solid oxide fuel cells. He is currently an Assistant Professor with the Department of Automotive Engineering, Yeungnam University, South Korea. His research interests include low-temperature SOFCs, thin film mechanics, nano/micro fabrications, and energy conversion devices. He received the Best Ph.D. Thesis Award.